Available online at www.sciencedirect.com
SCIENCE DIRECT®
ELSEVIER
International Journal of Mechanical Sciences 47 (2005) 545–569
International Journal of MECHANICAL SCIENCES
www.elsevier.com/locate/ijmecsci

Metal sandwich plates optimized for pressure impulses

John W. Hutchinson*, Zhenyu Xue

Division of Engineering and Applied Sciences, Harvard University, Pierce Hall, Cambridge, MA 02138, USA

Received 2 August 2004; accepted 4 October 2004
Available online 23 March 2005

Abstract

Survival of a plate against an intense, short duration impulsive loading requires the circumvention of failure modes, including those associated with excessive overall deflection and shear-off at supports and webs. All-metal sandwich plates have distinct advantages over comparable weight monolithic plates, especially for intense water loadings. A recently developed mechanics of dynamically loaded sandwich plates by N. A. Fleck and V. S. Deshpande is extended and modified to address the problem of the minimum weight design of plates of given span that must sustain a uniformly distributed impulsive wave in air or water environments. Requirements for core crushing strength and energy absorption are discussed, as are conditions governing shear-off of the face sheet. Dimensionless parameters governing optimal designs are identified. Specific results are presented for plates with square honeycomb cores outlining trends for the best performance that can be achieved and the optimal distribution of mass between faces and core. Optimally designed sandwich plates can sustain water shocks that are two to three times as large monolithic plates of the same mass and material. The model is used to discuss a number of issues relevant to the design of effective metal sandwich plates, including differing requirements for air and water environments, face sheet shear-off resistance, the role of core strength, and the relation between small-scale tests and full-scale behavior.
© 2005 Elsevier Ltd. All rights reserved.

Keywords: Impulsive loading; Sandwich plates; Honeycomb cores; Optimal design

*Corresponding author. Tel.: +1 617 495 2848; fax: +1 617 495 9837.
E-mail address: hutchinson@husm.harvard.edu (J.W. Hutchinson).

0020-7403/$ - see front matter © 2005 Elsevier Ltd. All rights reserved.
doi:10.1016/j.ijmecsci.2004.10.012

Nomenclature

B	in-plane spacing of webs of square honeycomb core
c_w	sound speed in water
C_L	Eq. (23)
D_{crit}	maximum allowed normalized deflection, δ/L
E	Young's modulus
f, f_T, f_B, f_F	dimensionless functions defined in Section 2
h, h_c, h_f	thickness of the solid plate, core webs and face sheets, respectively
H, $\bar{H}$	thickness of undeformed and deformed core, respectively
$I_0 = p_0 t_0$	momentum/area of incident pressure pulse
I_T	total momentum/area transmitted to sandwich plate and added water mass
I_F	momentum/area transmitted to front face and added water mass
I_B	momentum/area transmitted to core and back face
KE_I, KE_{II}	kinetic energy/area at end of Stages I and II
$\ell_w = c_w t_0$	characteristic thickness of incident pressure pulse in water
L	half-width of plate
m, m_c, m_f	mass/area of solid plate, core and face sheet
m_w	mass/area of added water layer
M	total mass/area of plate: $m = \rho h$ or $2m_f + m_c = \rho h_f(2+\mu)$
N	strain hardening exponent in shear-off analysis
p, p_0	pulse pressure, peak pressure of free-field pulse
r_w	ratio of mass/area of added water layer to face sheet, m_w/m_f
R_c	relative density of core
t_0	characteristic time of incident pressure pulse
t_C	time at the onset of cavitation and the end of Stage I
t_{II}, t_{III}	time at the end of Stages II and III
V_0	velocity of the solid plate (or top face) at end of Stage I
W_c^P	plastic work dissipated by core crushing in Stage II
W_{III}^P	plastic work dissipated in Stage III
β	fluid-structure interaction parameter
Γ_{SH}	shear-off resistance
δ, δ_{front}	deflection of plate or back face, deflection of front face
$\bar{\varepsilon}_c$	average crushing strain of core in Stage II
ε_{eff}^P	effective plastic strain in shear-off analysis
λ_c, λ_S	factors governing strength of core in crush and stretch
μ	measure of relative mass in core, m_c/m_f,
ρ, ρ_w	density of base metal, density of water
σ_Y	yield strength of base metal
σ_Y^c	yield strength of core in crush
σ_{ref}	reference strength in shear-off analysis, $\sigma_Y\ (E/\sigma_Y)^N$

1. Introduction

The superior performance of sandwich plates relative to solid plates of equal mass for shock loading in water is due to three factors: (i) energy absorption by the sandwich core, (ii) the substantial bending strength of a sandwich plate, and (iii) lower momentum transfer to a sandwich plate from the water pulse. More than half of the kinetic energy initially imparted to a sandwich plate by a uniformly distributed impulsive pressure loading must be absorbed by the core, whether the pressure pulse is in air or water. Consequently, concepts related to energy absorption in metal structural components [1] are central to the effective design of sandwich plates against intense short duration pressure loadings. The major advantage of sandwich plates relative to solid plates is against water pulses because significantly less momentum is acquired by the sandwich due to wave interaction between the water and the face sheet towards the pulse [2–7]. Recent theoretical work [4,5,7] has provided preliminary assessments of the benefits to be expected from sandwich design in a water environment. Moreover, it has been demonstrated that finite element methods are capable of accurately simulating most details of the structural response in a series of experiments on sandwich plates with square honeycomb cores struck by metal foam projectiles [8].

This paper continues the examination of all-metal sandwich plates by focusing on optimal performance under uniform impulsive pressure loading. The primary purposes are to identify the dominant features governing the most effective designs and to provide in broad outline the best performance that can be expected. We adopt the approximate analytical approach developed by Fleck and Deshpande [4] that separates the dynamic response of the plate into three stages: Stage I, fluid-structure interaction; Stage II, core crushing; and Stage III, overall bending and stretching. That analysis is extended in several respects. Most importantly, an enhancement of Taylor's [2] treatment of fluid-structure interaction is presented is Section 2 that accounts for the yield strength of the core. It will be shown that the enhanced fluid-structure interaction results become important when optimal designs are sought. Shear-off of the face sheet (Section 4), either at the supports or at core webs, is an additional failure mode that becomes important when optimal configurations are sought. The core of a sandwich plate must absorb more than half of the initial kinetic energy imparted to the plate (Section 3). For this reason, most attention here is directed towards square honeycomb cores. Earlier work [5] has shown that these cores are particularly effective in this application, combining high crushing strength and energy absorption with good in-plane stretch resistance. Optimization of sandwich plates highlights a small set of dimensionless parameters characterizing performance and design. Comparisons with equal mass solid plates will be made, and outstanding issues concerning the design of plates against intense impulsive loads will be discussed.

Overall trends relating the primary design variables for sandwich and solid plates to impulse level for both air and water environments will be sought. Relatively simple analytical approximations afforded by the neglect of strain hardening, material strain-rate effects, together with simplifications of the deformation response of the type employed by Fleck and Deshpande, allow this objective to be achieved. Full three-dimensional finite element simulations will be required for more accurate refinements [5,7–9].

2. Extended fluid-structure interaction in Stage I

Taylor's [2,3] one-dimensional analysis of the momentum transferred to a solid plate by a pressure pulse propagating towards it through a fluid medium can be used to estimate the momentum transferred to the face sheet of a sandwich plate towards the shock as long as the core strength is small and the pulse time is sufficiently short. However, if the core offers significant resistance to the motion of the face sheet, more momentum is transferred to the sandwich plate than Taylor's formula predicts. Moreover, the location of the plane where the onset of cavitation occurs shifts from the fluid-plate interface to a point within the fluid, giving rise to a layer of added water mass moving with the same velocity as the face sheet. Earlier efforts to seek the optimal distribution of mass between faces and core for water pulses based on the Taylor formula led to the conclusion that an optimal sandwich plate would have most of its mass in the core with unacceptably thin faces [4]. The enhanced Taylor analysis presented below is one of the ingredients essential to a more realistic optimization analysis, as will be illustrated.

The model analyzed in the Appendix idealizes the core as perfectly plastic with compressive yield stress, σ_Y^c, and the face sheet as a plane of concentrated mass per unit area, m_f. The fluid has density, ρ_w, and wave speed, c_w. As in Taylor's analysis, the free-field pressure pulse approaching the plate is of exponential form with time dependence, $p = p_0 e^{-t/t_0}$ where t_0 will be referred to as the pulse time and p_0 as the peak pressure. With x measured from the face sheet and $x<0$ in the fluid, the spatial dependence of the incident pulse at the instant it first hits the face is $p = p_0 e^{x/\ell_w}$ with $\ell_w = c_w t_0$. The momentum/area of the free-field pulse is $I_0 = \int p\,dt = p_0 t_0$. The following formulae provide the lowest order influence of σ_Y^c on the momentum transferred to the plate and the other quantities of interest at the *onset of cavitation* when the plate and added water layer separate from the bulk of the fluid.

The total momentum/area transferred to the sandwich plate (Fig. 1a), including the momentum of the added water layer, is

$$\frac{I_T}{I_0} \equiv f_T = 2f(\beta) + 1.27\,\frac{\sigma_Y^c}{p_0}\,(1 - f(\beta)) \tag{1}$$

with

$$f(\beta) = \beta^{\beta/(1-\beta)} \quad \text{and} \quad \beta = \rho_w \ell_w / m_f. \tag{2}$$

The ratio, $r_w = m_w/m_f$, (Fig. 1b) of the added layer of water mass/area, m_w, to the mass/area of the face sheet is

$$r_w = 0.71\beta\,\frac{\sigma_Y^c}{p_0}. \tag{3}$$

The momentum/area transferred to the core and the back face sheet (Fig. 1c) is

$$\frac{I_B}{I_0} \equiv f_B = 3.64\,\frac{\sigma_Y^c}{p_0}\,f(\beta). \tag{4}$$

Consequently, the momentum/area acquired by the front face sheet and the added water layer at the onset of cavitation is $I_F/I_0 \equiv f_F = f_T - f_B$. The time, t_C, at the onset of cavitation, measured

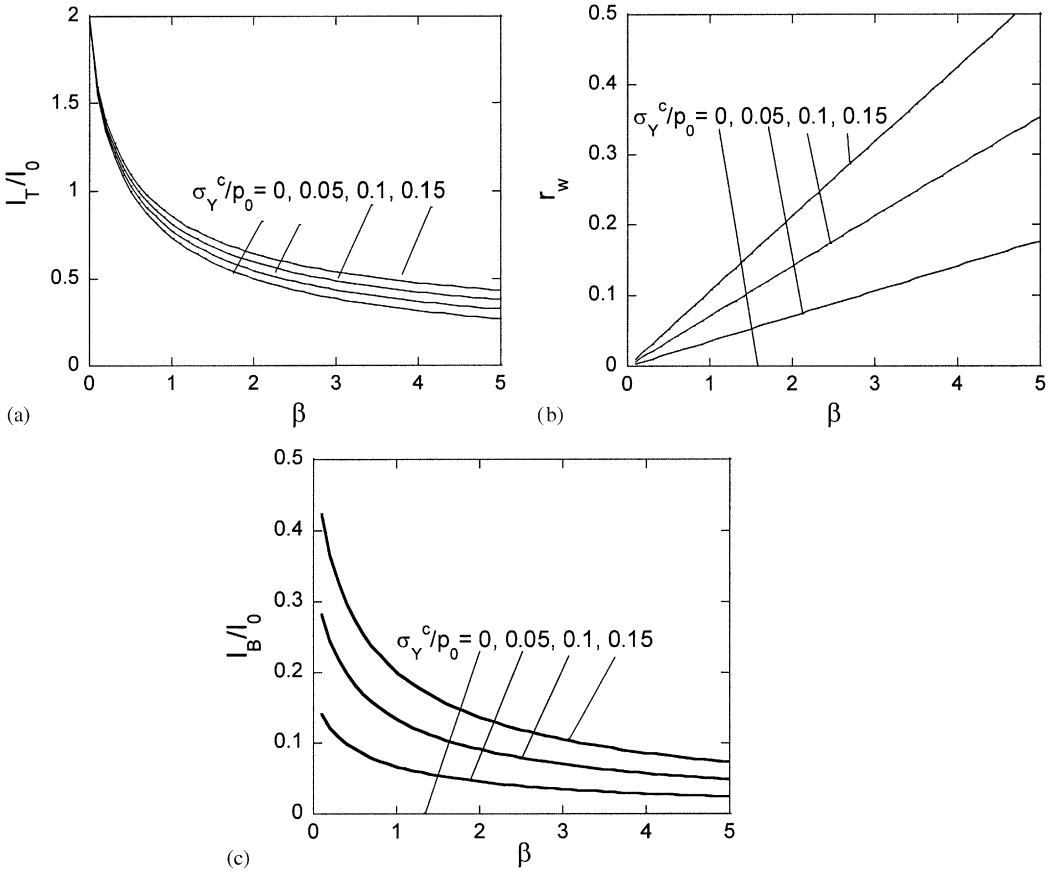

Fig. 1. Extended fluid–structure interaction trends at onset of cavitation accounting for strength of the core. (a) Total momentum/area acquired by sandwich plate, including added water mass. (b) Ratio of added water mass/area to mass/area of face sheet. (c) Momentum/area acquired by core and back face.

from the instant when the pulse first hits the front face, is given by $t_C/t_0 = \ln \beta/(1-\beta)$ when $\sigma_Y^c/p_0 = 0$ and is only slightly altered for non-zero σ_Y^c/p_0.

The above formulae, which include only linear terms in σ_Y^c/p_0, provide highly accurate approximations to the results for the model in the Appendix for $\sigma_Y^c/p_0 < 0.15$. The formulas will be used in the following sections to prescribe initial velocities for solid and sandwich plates. Taylor's result for a single solid plate ($I/I_0 \equiv f_T = 2f(\beta)$ with $\beta = \rho_w \ell_w/m$) is retrieved with $m_f = m$, $\sigma_Y^c/p_0 = 0$ and $r_w = 0$. When the fluid transmitting the pulse is air, β is very small. Here, for a sandwich plate in an air blast, the limit $\beta \to 0$ will be used such that $I_T = 2I_0$ with $f_T = 2$, $f_B = 0$, $f_F = 2$ and $r_w = 0$. For intense pulses these estimates are altered by nonlinear compressibility of the air, not accounted for in either the Taylor analysis or the present analysis, and the momentum/area acquired by a plate can be greater than $2I_0$. Nevertheless, these formulae allow one to make meaningful comparisons of solid and sandwich plates. If desired, results presented later for responses in air may be converted by replacing $2I_0$ with more accurate estimates of the impulse/area transmitted to the plate by the pulse.

Use of the above formulae rests on the tacit assumption that the cavitation plane continues to separate the bulk of the fluid from the plate after the onset of cavitation. A more detailed analysis [6] of the fluid response reveals that the cavitated region subsequently collapses resulting in additional transfer of momentum by the bulk of the fluid to the plate. However, that analysis indicates that this additional momentum is generally a small fraction of the momentum in the plate at the onset of cavitation if $\sigma_Y^c/p_0 < 0.15$ and if the free-field impulse level does not fully compact the core (see Appendix). Both conditions are met for the sandwich plates considered here, and, thus, the extended formulae, (1)–(4), are expected to provide reasonably accurate approximations of fluid-structure interaction for partitioning the total momentum transferred to the plate into the portion acquired by the front face sheet and added water layer and that acquired by the core/face sheet combination behind it.

3. Energy absorption requirements of the core in Stage II

The elements of the plate are set into motion at the instant of cavitation with velocities that will be derived from the results of Section 2. The analysis of the plate response employs the three stages of response identified by Fleck and Deshpande [4]: Stage I ($0 < t < t_C$) ending at the onset of cavitation, Stage II ($t_C < t < t_{II}$) comprising the period of core crush and ending when all components of the plate have acquired the same velocity, and Stage III ($t_{II} < t < t_{III}$) comprising the period when energy not dissipated in Stage II is absorbed in overall bending and stretching of the plate. The period, t_C, characterizing Stage I is on the order of the pulse time, t_0. For stage II, $t_{II} \approx I_T/2\sigma_Y^c \approx (p_0/\sigma_Y^c)t_0$. The total response time for a heavy impulse is $t_{III} \approx L\sqrt{\rho/\sigma_Y}$ where L is an in-plane dimension of the plate with ρ and σ_Y as the density and yield strength of the plate material [9]. The three time scales are required to be well separated in the Fleck–Deshpande approach. This appears to be a good assumption for large-scale plates (in-plane dimension on the order of a meter) with relatively strong cores that are subject to loadings characteristic of air and water pulses with $t_0 \approx 10^{-4}$ s [4,5,7].

At the end of Stage I, the kinetic energy/area in the front face sheet and the added water mass is $I_F^2/[2(m_f + m_w)]$, while that in the core and the back face sheet is $I_B^2/[2(m_f + m_c)]$, where m_c is the mass/area of the core. Here, as an approximation, a uniform velocity in the core and the back face sheet at cavitation has been assumed.[1] Thus, the total kinetic energy/area at the end of Stage I is

$$KE_I = \frac{I_F^2}{2(m_f + m_w)} + \frac{I_B^2}{2(m_f + m_c)}. \tag{5}$$

The response in the interior of the plate during Stages I and II is assumed to be unaffected by supports at the perimeter of the plate, consistent with the supposition $t_{II} \ll t_{III}$. Thus, under a uniformly distributed pulse, motion away from the supports is one-dimensional and momentum is conserved. When core crushing is complete at the end of Stage II, the faces sheets, core and added water layer move at uniform velocity, neglecting elastic vibrations. By momentum conservation,

[1] Deshpande and Fleck's [6] analysis accounts for non-uniform deformation of the core during Stages I and II. The effect of assuming a uniform velocity in the core and the back face at the end of Stage I in the present analysis introduces little error because most of kinetic energy is in the front face.

the kinetic energy/area of the sandwich plate and added water mass at the end of Stage II is

$$KE_{II} = \frac{I_T^2}{2(2m_f + m_c + m_w)}. \tag{6}$$

The kinetic energy dissipated in Stage II by core crushing, $KE_I - KE_{II}$, is a large fraction of the initial kinetic energy imparted to the plate. To see this, one can use the results of the previous section to obtain

$$\frac{KE_I - KE_{II}}{KE_I} = \frac{f_F^2/(1+r_w) + f_B^2/(1+\mu) - f_T^2/(2+\mu+r_w)}{f_F^2/(1+r_w) + f_B^2/(1+\mu)}. \tag{7}$$

This ratio depends on three parameters:

$$\frac{\sigma_Y^c}{p_0}, \quad \mu \equiv \frac{m_c}{m_f}, \quad \beta \equiv \frac{\rho_w \ell_w}{m_f} = (2+\mu)\,\frac{\rho_w \ell_w}{M}, \tag{8}$$

where $M = 2m_f + m_c$ is the total mass/area. The dimensionless parameter, $M/\rho_w \ell_w$, is central in the development which follows. For pulses with $t_0 = 10^{-4}$ s in water, $\ell_w \cong 0.15$ m and $\rho_w \ell_w \cong 150\,\mathrm{kg/m^2}$ such that $M/\rho_w \ell_w = 1$ corresponds to a sandwich plate having the equivalent mass/area of a 2 cm thick plate of steel. If the effect of σ_Y^c/p_0 is neglected, such that $f_B \cong 0$ and $r_w \cong 0$, ratio (7) becomes

$$\frac{KE_I - KE_{II}}{KE_I} \cong \frac{1+\mu}{2+\mu}, \tag{9}$$

which is independent of $M/\rho_w \ell_w$ and thus valid in air or water. This estimate is approximately valid for all sandwich plates (Fig. 2).

As noted above, the core must be designed to dissipate more than one-half, and, typically, about two-thirds, of the initial kinetic energy imparted to the sandwich plate by a substantial pulse. We continue with the idealized model of a perfectly plastic core with rate-independent yield strength σ_Y^c. The average crushing strain of the core at the end of Stage II is denoted by $\bar{\varepsilon}_c =$

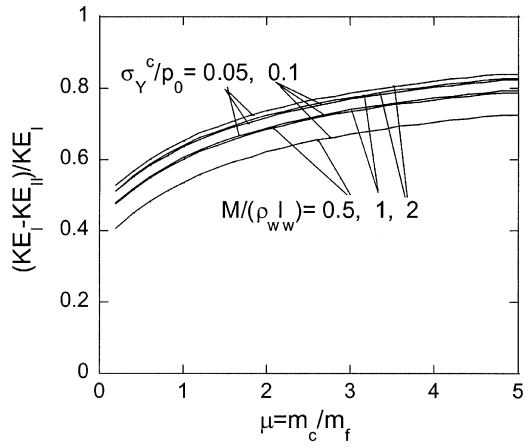

Fig. 2. Ratio of kinetic energy/area absorbed in core in Stage II to kinetic energy/area acquired in Stage I.

$\Delta H/H$, with H and $\bar{H}$ as the initial and deformed core thickness, respectively, and $\Delta H = H - \bar{H}$. The plastic energy/area dissipated by the core is $W_c^P = \sigma_Y^c \bar{\varepsilon}_c H$. Introduce the relative density of the core, R_c, defined as the fractional volume of the core occupied by the material, such that $m_c = \rho R_c H$ where ρ is the base material density. It is convenient to introduce a 'core compression strength factor', λ_c, defined in terms of the material yield strength, σ_Y, as

$$\sigma_Y^c = \lambda_c R_c \sigma_Y. \tag{10}$$

Assuming yielding occurs prior to elastic buckling in the core (see Section 8.5), a square honeycomb core has $\lambda_c = 1$, while a tetragonal truss core has $\lambda_c = 2/3$. Weaker cores, such as foam metal cores, can have $\lambda_c \approx 0.1$. This simple expression does not account for strength variation as the core crushes, but they are adequate for present purposes.

The crushing strain is obtained by equating the plastic dissipation in the core W_c^P to the kinetic energy loss in Stage II, $KE_I - KE_{II}$. To obtain $\bar{\varepsilon}_c$, note that $W_c^P = \sigma_Y^c \bar{\varepsilon}_c H$ can be written as $W_c^P = \lambda_c (M\sigma_Y/\rho)\bar{\varepsilon}_c \mu/(2+\mu)$, and then express $KE_I - KE_{II}$ in terms of the extended Taylor formulae using Eqs. (5) and (6):

$$\bar{\varepsilon}_c = \left(\frac{I_0}{\sqrt{\sigma_Y/\rho M}}\right)^2 Q, \tag{11}$$

where

$$Q = \frac{(2+\mu)^2}{2\mu\lambda_c}\left[\frac{f_F^2}{1+r_w} + \frac{f_B^2}{1+\mu} - \frac{f_T^2}{2+\mu+r_w}\right]. \tag{12}$$

Eq. (11) for the crushing strain will be employed in the optimization of the square honeycomb core sandwich plates and in Section 8 in connection with a general discussion of core strength requirements.[2]

4. A criterion for face sheet shear-off

Among other failure concerns, the front face sheet (towards the pulse) must not shear-off, either at the supports at the edge of the plate or where it is supported at the core webs. If shear-off occurs, it does so very early in the history of the plate response prior to significant core crush and overall bending and stretching. In this section, results on shear-off from Jones [10] and Xue [11] will be used to identify a criterion governing shear-off. A solid plate or face sheet of thickness, h, density, ρ, and tensile stress–strain behavior in the plastic range given by $\sigma = \sigma_Y(E\varepsilon/\sigma_Y)^N \equiv \sigma_{ref}\varepsilon^N$ is considered. The plate is clamped at its supports and is set in motion at $t = 0$ with uniform velocity, V_0.

An analysis of shear-off for a perfectly plastic plate ($N = 0$) has been presented [10] based on an approximate yield condition for plates that decouples transverse shearing and bending. A finite width plate was considered with simply supported end conditions. For the idealized yield model, shear-off is measured by a shearing displacement normal to the beam at the support, w_{SH}. For all

[2]The core strain occurring in Stage I is generally much smaller than Eq. (11), which applies to Stage II. It will be neglected in determining the deformed thickness of the core, $\bar{H}$, used in the Stage III analysis.

but very narrow plates, the extent of shear-off is independent of the plate width since the deformation is confined to the immediate vicinity of the end, as illustrated in the insert in Fig. 3. Repeating the analysis in [10] for a clamped, semi-infinite plate, we find that the shear-off displacement is $w_{SH} = 9\rho h V_0^2/8\sigma_Y$ and that it is achieved at $t_{SH} = 9\rho h V_0/\sigma_Y$. For $t > t_{SH}$, no further shearing displacement occurs. For full-scale plates and velocities of interest here, t_{SH} is on the order of 10^{-4} s, and therefore on the order of the pulse time, t_0. As mentioned earlier, if it occurs, shear-off takes place early in the deformation history.

A finite strain analysis of shear-off using a finite element analysis with detailed meshing through the thickness of the plate has been carried out [11] considering both elastic-perfectly plastic behavior and the strain hardening behavior noted above for materials with a Mises yield surface. In the refined analysis, no shear displacement at the support, w_{SH}, occurs even in the absence of strain hardening. Instead, large plastic shear strains occur at the plate/support intersection as seen

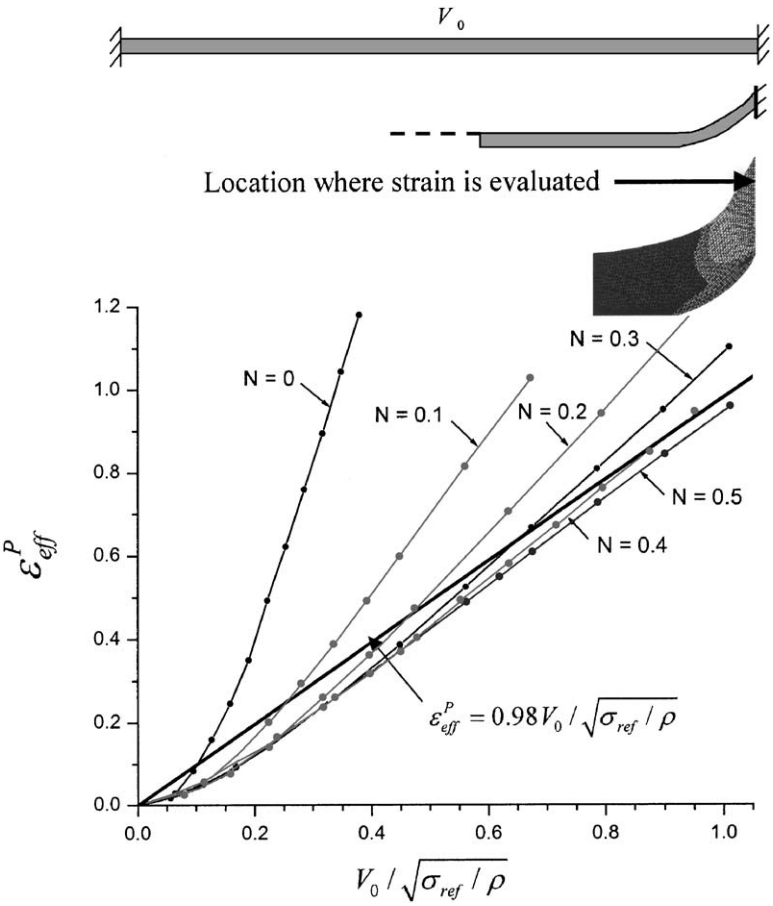

Fig. 3. Shearing in solid plate at clamped support measured by effective plastic strain at the top corner as dependent on initial velocity, V_0, imparted to plate [11]. The inserts show deformation at the end of the period when the plate is susceptible to intense shearing at the supports prior to any overall bending and stretching. Further details of the strain distribution are discussed in the text.

in the insert in Fig. 3. Across the plate thickness at the intersection there is about a factor of two variation of the plastic shear strain. The largest strain occurs at the bottom corner where an acute vertex develops under finite deformation, while the minimum strain occurs near the top where the corner becomes obtuse with deformation. A selection of results [11] for the minimum shear strain in the plate at the clamped support (the strain occurring near the top of the intersection) is presented in Fig. 3. The shear strain, as measured by the effective plastic strain, ε^P_{eff}, is plotted as a function of $V_0/\sqrt{\sigma_{ref}/\rho}$ for various values of the strain hardening exponent, N. The average strain across the intersection is roughly 30% larger than the minimum strain plotted. In Ref. [11] it is established that $V_0/\sqrt{\sigma_{ref}/\rho}$ captures all the parametric dependence, and, specifically, it is shown there is no additional dependence on h, σ_Y or E. At small values of $V_0/\sqrt{\sigma_{ref}/\rho}$ the dependence on V_0 is not linear. However, at larger strains of relevance to shear-off and for moderate to heavy strain hardening, the plastic strain in Fig. 3 can be approximated as

$$\varepsilon^P_{eff} \cong 0.98 V_0/\sqrt{\sigma_{ref}/\rho}. \tag{13}$$

The condition used to exclude shear-off in the sequel is taken as

$$V_0/\sqrt{\sigma_Y/\rho} \leqslant \Gamma_{SH}, \tag{14}$$

where Γ_{SH} is a parameter characterizing resistance to shear-off. Limited evidence available for identifying Γ_{SH} will be discussed in the next section. The extension of Jones' analysis quoted above would also lead to a criterion based on the combination $V_0/\sqrt{\sigma_Y/\rho}$ if a value of w_{SH}/h were identified as being critical to shear-off.

Shear-off of the face sheet is also a possibility where it is attached to a core web, if the web is sufficiently strong. For a specific example, consider a square honeycomb core (Fig. 4a) where the core webs have thickness, h_c, and in-plane spacing, B, equal to the core thickness, H. For webs and faces made of a perfectly plastic material with a Mises yield surface, it is readily shown that the core web will yield in compression before the face sheet can yield in shear if $h_c \leqslant 2h_f/\sqrt{3}$, or, equivalently, if

$$\mu \equiv \frac{m_c}{m_f} \leqslant \frac{4}{\sqrt{3}} \quad \text{(square honeycomb core, } B = H\text{)}. \tag{15}$$

Thus, even if an end support is designed to avoid rigid clamping of the face sheet, the face may shear-off where it is attached to the core webs if both Eqs. (14) and (15) are violated.

5. Equations governing bending and stretching of plates in Stage III

The kinetic energy/area of the plate at the end of Stage II, KE_{II} in Eq. (6), must be dissipated by bending and stretching of the plate in Stage III. Solid and sandwich construction will be compared for plates of the same material and having the same mass/area, M. As already emphasized, the base material is idealized to be rate-independent and perfectly plastic with yield stress, σ_Y. The plate has width $2L$, is fully clamped at both ends, and is imagined to be of infinite extent in the y-direction. The pulse hitting the plate is taken as uniform such that at the beginning of Stage III, KE_{II} is uniformly distributed over the plate. To estimate the deflection produced by this kinetic energy, a relatively simple estimate of the energy dissipated in bending and stretching is obtained

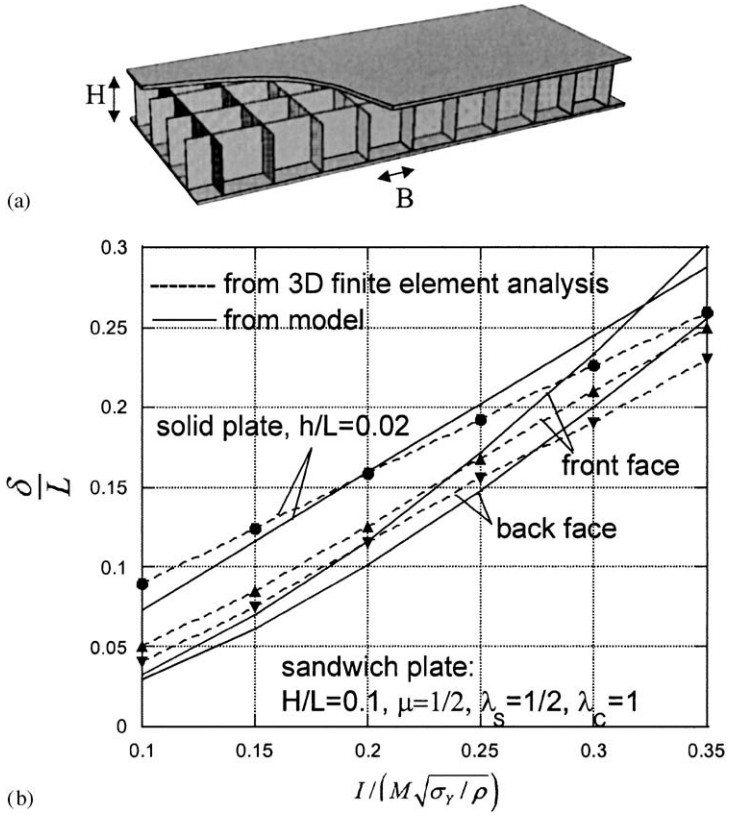

Fig. 4. (a) Sandwich plate with square honeycomb core. (b) Comparison of model predictions with results from three-dimensional finite element computations [5]. An impulsive loading corresponding to an initial momentum/area, I, is applied to each plate. See text for specification of details.

using approximations for the deformation that neglect details of the dynamics. The energy dissipated by plastic deformation is sought in terms of the center deflection of the plate.

A solid plate of thickness h and mass/area $M = \rho h$ is considered first. The limit bending moment/length of the plate is $m_Y = \sigma_Y h^2/4$. Under quasi-static uniform load, hinges form at each end of the plate and at the center. The plastic work per length in the y-direction is $8m_Y\delta/L = 2\sigma_Y h^2\delta/L$ where δ is the deflection at the center of the plate ($\sigma_Y h^2\delta/L$ for a plate simply-supported at it ends). Hinges relax the constraint on the slope at its ends when stretch becomes dominant. To estimate the plastic work in stretching, assume a deflection shape $w = \delta[1 - (x/L)^2]$ with x measured from the center of the plate. The average stretching strain in the plate is $\bar{\varepsilon} = 2(\delta/L)^2/3$ and the plastic work/length dissipated in stretch is $2\sigma_Y \bar{\varepsilon} hL$. The average plastic work per area dissipated in Stage III, W^P_{III}, is estimated by summing the two contributions given above:

$$W^P_{III} = \frac{2}{3}\sigma_Y h\left(\frac{\delta}{L}\right)^2 + \sigma_Y h\frac{h}{L}\frac{\delta}{L}. \tag{16}$$

Bending makes the dominant contribution for $\delta < h$ while stretch dominates for $\delta > h$. The present estimate ignores details of the dynamic spread of plastic hinges during the bending phase of the deformation accounted for in the estimate obtained by Fleck and Deshpande [4]. Nevertheless, Eq. (16) provides a good approximation to the overall energy dissipation since it depends only weakly on deformation history, as will be illustrated by comparisons with accurate numerical results.

A similar analysis for the clamped sandwich plate gives $8\sigma_Y \bar{H} h_f(\delta/L)$ as the work/length dissipated in bending (bending dissipation in the core is neglected and $\bar{H} = H(1-\bar{\varepsilon}_c)$ is the core thickness at the end of Stage II), and $2\sigma_Y h_f(2+\lambda_S\mu)\bar{\varepsilon}L$ as the work/length dissipated in stretch. Core dissipation in stretch is included through the factor λ_S that measures the fraction of the core material aligned such that it resists stretch in the x-direction, i.e., $\sigma_Y^S = \lambda_S R_c \sigma_Y$. A square honeycomb core (Fig. 4a) has $\lambda_S = 1/2$, while a truss core has $\lambda_S = 0$. The plastic work/area dissipated in Stage III in the sandwich plate is

$$W_{III}^P = \frac{2}{3}\sigma_Y h_f(2+\lambda_S\mu)\left(\frac{\delta}{L}\right)^2 + 4\sigma_Y h_f \frac{\bar{H}}{L}\frac{\delta}{L} \tag{17}$$

with $\bar{H} = H(1-\bar{\varepsilon}_c)$. For the sandwich plate, the deflections of the front (towards the shock) and back faces are given by $\delta_{front} = \delta + \bar{\varepsilon}_c H$ and $\delta_{back} = \delta$, respectively.

5.1. Solid plate

The equation for the plate deflection is obtained by equating W_{III}^P in Eq. (16) to KE_{II}, accounting for an air or water environment in the evaluation of KE_{II}, i.e.,

$$\frac{1}{8}\left(\frac{\delta}{L}\right)^2 + \frac{1}{2}\frac{h}{L}\frac{\delta}{L} = f(\beta)^2\left(\frac{I_0}{M\sqrt{\sigma_Y/\rho}}\right)^2 \tag{18}$$

with $M = \rho h$, and where $\beta = \rho_w \ell_w / M$ in water and $\beta = 0$ in air. Condition (14) for avoiding shear-off is re-written using $\rho h V_0 = 2f(\beta) I_0$:

$$2f(\beta)\frac{I_0}{M\sqrt{\sigma_Y/\rho}} \leqslant \Gamma_{SH}. \tag{19}$$

Plate deflection will be constrained such that

$$\delta/L \leqslant D_{crit}. \tag{20}$$

Equivalently, the overall stretching strain is constrained by $\bar{\varepsilon} \leqslant 2D_{crit}^2/3$. In the numerical examples, specific values of D_{crit} and Γ_{SH} will be prescribed. They must be chosen to avoid stretching and shear fracture or, in the case of D_{crit}, unacceptably large deflections.

5.2. Sandwich plate

Equating W^P_{III} in Eq. (17) to KE_{II} gives the deflection of the back face sheet as

$$\frac{4(2+\mu+r_w)}{(2+\mu)^2}\left[\frac{(2+\lambda_S\mu)}{3}\left(\frac{\delta}{L}\right)^2+2\,\frac{H}{L}\,(1-\bar{\varepsilon}_c)\,\frac{\delta}{L}\right]=f_T(\beta)^2\left(\frac{I_0}{M\sqrt{\sigma_Y/\rho}}\right)^2 \tag{21}$$

with $M=\rho h_f(2+\mu)$ and where $\beta=(2+\mu)\rho_w\ell_w/M$ in water and $\beta=0$ in air. The crushing strain, $\bar{\varepsilon}_c$, is given by Eqs. (11) and (12), and the deflection of the front face is $\delta_{front}=\delta+\bar{\varepsilon}_c H$. The shear-off constraint (14) is expressed using $\rho h_f(1+r_w)V_0=I_F$:

$$\left(\frac{2+\mu}{1+r_w}\right)f_F(\beta)\,\frac{I_0}{M\sqrt{\sigma_Y/\rho}}\leqslant\Gamma_{SH}. \tag{22}$$

The functions f_T, f_F, f_B and r_w defined in Section 2 depend on both β and σ^c_Y/p_0. An expression for σ^c_Y/p_0 is obtained from Eq. (10) as

$$\frac{\sigma^c_Y}{p_0}=\frac{\lambda_c\mu}{(2+\mu)}\left(\frac{M\sqrt{\sigma_Y/\rho}}{I_0}\right)\frac{L}{H}\,C_L\quad\text{with } C_L=\sqrt{\frac{\sigma_Y}{\rho}}\,\frac{t_0}{L}. \tag{23}$$

Here, L has been introduced since H/L is one of two design variables. The other is μ; C_L is fixed in the optimization process. Limits on deflection and shear of the front face sheet, D_{crit} and Γ_{SH}, will be taken as the same as those for the solid plate.

5.3. Comparison with detailed finite element results

Fig. 4b presents a comparison of results for solid and sandwich plates with square honeycomb cores from Eqs. (18) and (21), respectively, with full three-dimensional finite element simulations for the same plates in Ref. [5]. The material has $\rho=8000\,\mathrm{kg/m^3}$ and $\sigma_Y=205\,\mathrm{MPa}$, and is taken to be perfectly plastic in the present model but with moderate strain hardening ($N=0.2$) in the finite element simulations. Both plates have $L=1\,\mathrm{m}$ and $M/\rho L=0.02$ (corresponding to $M=160\,\mathrm{kg/m^2}$ and $h/L=0.02$). The sandwich plate has $\mu=1/2$, $H/L=0.1$, and $B/H=1$ (corresponding to $R_c=0.04$). In the model, $\lambda_c=1$ and $\lambda_S=1/2$. The finite element simulations were intended to model air pulses and they were carried out by imposing a momentum/area, I, at $t=0$ as initial velocities $V_0=I/m$ on the solid plate and $V_0=I/m_f$ on the top face sheet of the sandwich plate. These initial conditions are reproduced in the present model in Eqs. (18) and (21) by taking $f_T=2, f_B=0, f_F=2, r_w=0$ with $I=2I_0$.

For an imposed momentum (Fig. 4b), the model underestimates the deflections in the lower range of impulses and overestimates the deflections in the upper range for both the sandwich plate and the solid plate. In the upper range impulse range, the model also overestimates the crushing of the core. In both respects, the model results are similar to those in Ref. [4]. Two sources of discrepancy are the neglect of strain hardening in the model, which becomes increasingly important at larger deflections, and dynamic strengthening of the core due to inertial effects that is also largest in the upper range of impulses [12]. For moderately large deflections, $\delta/L\approx 0.2$, of primary interest in this paper, the model predictions are within 10% of the more accurate results.

6. Optimal plates against impulses in air

The minimum weight/area of a *solid plate* required to sustain the free-field pulse I_0 in air is given by Eq. (18) subject to constraints specified by Eqs. (19)–(20). The only design parameter is h/L. Curves of $M/(I_0/\sqrt{\sigma_Y/\rho})$ versus D_{crit} for three values of h/L are given in Fig. 5. The influence of h/L, which is associated with the bending contribution to dissipation in Eq. (18), is small. Consequently, to a first approximation, the half-width of the solid plate, L, is not a significant factor in the dimensionless relation plotted.

Somewhat arbitrarily, the shear-off resistance in these simulations has been set at $\Gamma_{SH} = 1$, corresponding to a critical effective plastic strain, $(\varepsilon^P_{eff})_{crit} \approx 1$, at the supports. According to Eq. (19), with $f = 1$ and $\Gamma_{SH} = 1$, shear-off occurs if $I_0/(M\sqrt{\sigma_Y/\rho}) \geqslant 1/2$. The normalized impulse required to produce $D_{crit} = 0.2$ is $I_0/(M\sqrt{\sigma_Y/\rho}) \cong 0.14$ (c.f. Fig. 5), and this is only about one third the impulse needed to cause shear-off. Impulsive tests conducted on high strength aluminum strips [13] revealed that shear-off occurred only at impulses considerably higher than those required to produce deflections with $D_{crit} = 0.2$. Higher ductility materials should be able to sustain even larger initial impulses without shear-off. We have taken $\Gamma_{SH} = 1$ to be representative of materials with ample ductility, but definitive experiments are essential to establish shear-off resistance.

Results for *sandwich plates* with square honeycomb cores ($\lambda_c = 1$, $\lambda_S = 0.5$) evaluated using Eqs. (21)–(23) are also included in Fig. 5. Calculations were carried out for three values of C_L; note that $C_L = 0.0158$ applies for a typical steel ($\sigma_Y = 200\,\text{MPa}$, $\rho = 8000\,\text{kg/m}^3$) with $t_0 = 10^{-4}\,\text{s}$ and $L = 1\,\text{m}$. The results in Fig. 5 should be regarded as applicable to full-scale plates (i.e., meter scale); results for small-scale specimens will be discussed in Section 8.3. One set of results in Fig. 5 was obtained by minimizing M with respect to μ with H/L fixed at 0.1. The minimum has $\mu \cong 0.5$ over the entire range in good agreement with a more limited study [5]. Shear-off is not active. The

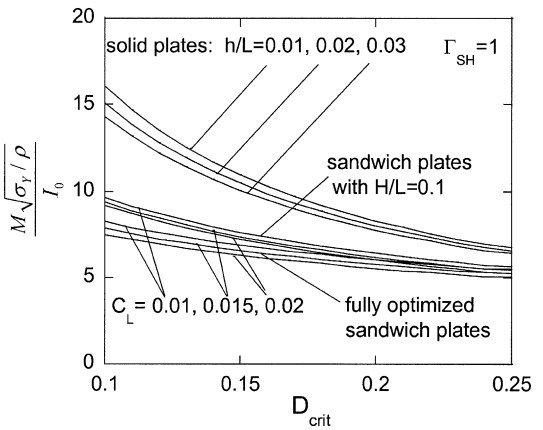

Fig. 5. Plot of normalized mass/area, $M\sqrt{\sigma_Y/\rho}/I_0$, of solid and sandwich plates with square honeycomb cores subject to *pulses in air* as a function maximum allowable normalized deflection. Two sets of results for the sandwich plates are presented: (i) plates optimized for minimum weight with respect to both H/L and μ with the result that $H/L \cong 0.3$ and $\mu \cong 1$ over the entire range; and plates with $H/L = 0.1$ optimized with respect to μ, with $\mu \cong 0.5$ over the entire range. The shear-off constraint is not active for any of these cases.

lower set of results is for a fully optimized plate with M minimized with respect to both μ and H/L. In these cases, too, shear-off is not active. Over the whole range of parameters shown, the fully optimized plates have $\mu \cong 1$ and $H/L \cong 0.3$. However, the minimum is very shallow, as evident from the fact that plates with $H/L = 0.1$ are only slightly heavier than fully optimal plates. The influence of the half-width of the plate on optimal value of $M\sqrt{\sigma_Y/\rho}/I_0$ is only through C_L and is evidently relatively weak over the range of this parameter shown.

For air blasts, roughly one third of the mass of the plate is in the core ($\mu \cong 1$) in the case of the optimally designed sandwich plate, while only about one fifth of the mass is in the core ($\mu \cong 0.5$) of the minimum weight plates constrained to have $H/L = 0.1$. The crushing strain, $\bar{\varepsilon}_c$, varies over the range considered, but is generally less than 20%. For maximum deflections less than $D_{crit} = 0.25$, a well-designed sandwich plate outperforms a solid plate having the same mass in an air blast. Moreover, the plate with $H/L = 0.1$ is almost as effective as the optimal plate with the much thicker core. If $D_{cril} > 0.3$, the advantage of the sandwich plate over the solid plate is lost in an air environment, since stretch dominates energy dissipation and the solid plate is superior in stretch to the sandwich. These trends are in good agreement with results from a three-dimensional finite element analysis [5] covering a restricted range of parameters.

7. Optimal plates against impulses in water

Due to fluid-structure interaction, an additional parameter arises in characterizing the response of plates in water: $\beta = \rho_w \ell_w/M$ and $\beta = (2+\mu)\rho_w \ell_w/M$ for the solid and sandwich plates, respectively. For a given free-field impulse, I_0, the minimum weight plate is sought. This is equivalent to seeking a plate of prescribed M that can sustain the largest free-field impulse. The latter view is the more convenient one, as can be seen in connection with the problem for the solid plate. With $\beta = \rho_w \ell_w/M$ prescribed, it is straightforward to obtain the largest value of $I_0/M\sqrt{\sigma_Y/\rho}$ satisfying Eqs. (18)–(20). For the choices $D_{crit} = 0.2$ and $\Gamma_{SH} = 1$, the outcome is plotted as $M\sqrt{\sigma_Y/\rho}/I_0$ in Fig. 6a and as $I_0/(\rho_w \ell_w \sqrt{\ell_Y/\rho})$ in Fig. 6b, in each case for $0 < M/\rho_w \ell_w \leqslant 3$.

With $M/\rho_w \ell_w$ and C_L prescribed, the two design parameters for the sandwich plate with a square honeycomb core ($\lambda_c = 1$, $\lambda_S = 0.5$) are μ and H/L. Eqs. (21)–(23) can be solved numerically in a straightforward fashion for the maximum I_0 for a given M with results plotted in Fig. 6. Results optimized with respect to μ for H/L fixed at 0.1 are shown along with results for plates optimized with respect to both μ and H/L. The values of C_L represent full-scale plates. In water blasts, the benefits of a well-designed sandwich plate over a solid plate of identical mass is substantial, as noted in earlier work [4,5,7]. Sandwich plates having $M/\rho_w \ell_w \leqslant 1$ can sustain free-field impulses about three times that of a comparable solid plate. As in the case for pulses in air, plates having $H/L = 0.1$ are also highly effective. This is significantly since other considerations may exclude deployment of sandwich plates as thick as $H/L \cong 0.3$.

Optimal designs for water environments allocate somewhat more mass to the core than those for air environments. The sandwich plates with $H/L = 0.1$ have about one third of their mass in the core ($\mu \cong 1$) and undergo crushing strains, $\bar{\varepsilon}_c$, that are less than 15%. The fully optimal plates with $H/L \cong 0.3$ have about one half of their mass in the core ($\mu \cong 2$) and have crushing strains less than 25%. Only the deflection constraint is active for the plates with $H/L = 0.1$, while both

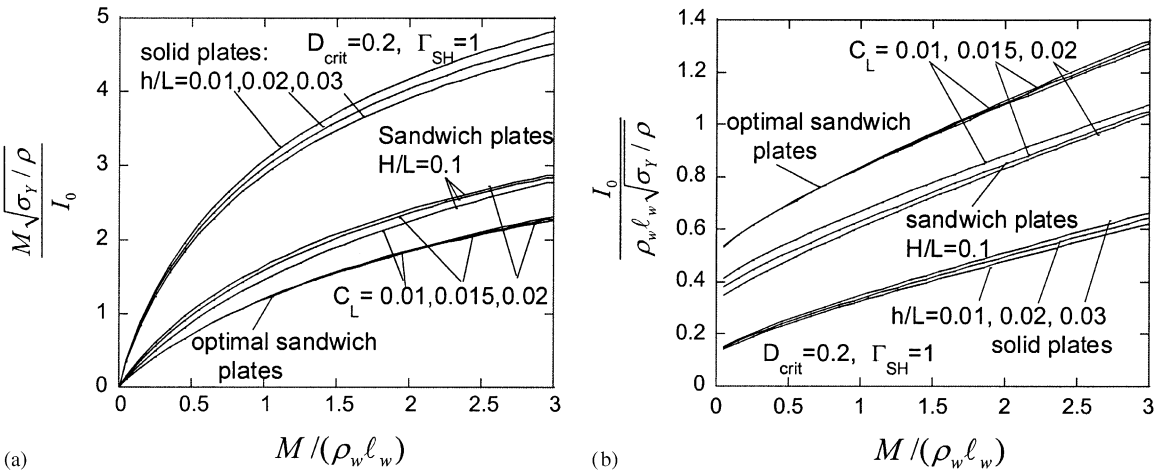

Fig. 6. Plots of (a) normalized mass/area and (b) normalized impulse for solid and sandwich plates with square honeycomb cores subject to *pulses in water* as a function $M/\rho_w\ell_w$ for $D_{crit} = 0.2$ and $\Gamma_{SH} = 1$. Two sets of results for the sandwich plates are presented. (i) Plates that are optimized for minimum weight with respect to both H/L and μ that have $H/L \cong 0.3$ and $\mu \cong 2$ over the entire range. Deflection and shear-off constraints are both active. (ii) Plates with $H/L = 0.1$ that are optimized with respect to μ, with $\mu \cong 1$ over the entire range. In this case, the shear-off constraint is not active.

deflection and shear-off are active for the fully optimal plates. *Curves computed with* ($H/L = 0.1$, $\mu = 1$) *and with* ($H/L = 0.3$, $\mu = 2$) *are nearly indistinguishable from those in Fig. 6.*

The finite impulse limit as $M/\rho_w\ell_w \to 0$, as seen in Fig. 6b, is a consequence of fluid-structure interaction. It requires explanation. According to the assumptions adopted here, plates of very small mass are able to sustain free-field impulses, I_0, below a critical level (c.f. Fig. 6b). This holds for the original Taylor fluid-structure analysis or the extended analysis. Indeed, the two analyses coincide for solid plates, and, for simplicity, behavior for the solid plate will be used to elucidate this unusual limit. As $M/\rho_w\ell_w \to 0$, the interaction parameter β becomes large such that the momentum/area transmitted to the solid plate becomes $I \to 2I_0/\beta = 2I_0/\beta(\rho h/\rho_w\ell_w)$. Thus, for very thin plates, the momentum/area acquired from a free-field impulse, I_0, is proportional to h and vanishes as $h \to 0$. The kinetic energy/area that must be dissipated also scales with h, as does W^P_{III}. Thus, very thin plates undergo a normalized deflection, δ/L, (and shear strains at the supports) which is independent of h. It follows, that as long as I_0 is below the limiting value in Fig. 6b, conditions for survival employed in this paper will be met even for very thin plates. Other constraints on performance will clearly be required for plates having very small $M/\rho_w\ell_w$. Elastic buckling of the core prior to plastic yielding gives rise to another reason to question the validity of the present predictions for small $M/\rho_w\ell_w$, as will be discussed in Section 8.5.

It is possible to present the results for the air and water environments in a unified setting that emphasizes the role of fluid-structure interaction in water blasts. To see this, replace the fluid-structure interaction parameter for water, by $M/\rho_{fluid}\ell_{fluid}$, where now $\rho_{fluid}\ell_{fluid}$ applies to any fluid medium. In Fig. 7, results, as measured by $M/(I_0/\sqrt{\sigma_Y/\rho})$, are plotted over an extensive

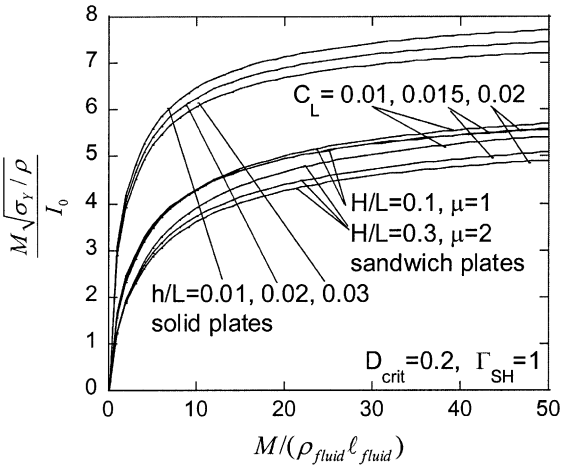

Fig. 7. Normalized mass/area, $M\sqrt{\sigma_Y/\rho}/I_0$, of solid and sandwich plates with square honeycomb cores subject to pulses in an arbitrary fluid as a function $M/\rho_{fluid}\ell_{fluid}$ for $D_{crit} = 0.2$ and $\Gamma_{SH} = 1$. The results apply to water with $\rho_{fluid}\ell_{fluid} = \rho_w\ell_w$ and to air for $M/\rho_{fluid}\ell_{fluid} \to \infty$.

range of $M/\rho_{fluid}\ell_{fluid}$. The curves apply to water with $\rho_{fluid}\ell_{fluid} = \rho_w\ell_w$, while the asymptotes of the same curves for large values of $M/\rho_{fluid}\ell_{fluid}$ apply to air.

To highlight the importance of the extended Taylor fluid–structure interaction formulae, we digress to present optimization results obtained using Taylor's original formula to determine the momentum acquired by the front face sheet towards the blast. In this simpler approach, the resistance of the core to the motion of the front face will be ignored and the core and back face will be taken to be motionless in Stage I. The following modifications apply: $f_T(\beta)$ is replaced by $2f(\beta)$ in (21), $f_F(\beta)$ is replaced by $2f(\beta)$ in (22) with $r_w = 0$, and $Q = 2(2+\mu)(1+\mu)f(\beta)^2/(\mu\lambda_c)$ in Eqs. (11) and (12). The half-width of the plate, L, is absent from these equations, apart from its appearance in the design variable, H/L. The optimization process leads to the results in Fig. 8, which have again been carried out both for H/L fixed at 0.1 and for full minimization with respect to both H/L and μ. The trends in Fig. 8 for the normalized mass of the plate, $M\sqrt{\sigma_Y/\rho}/I_0$, are not very different from those in Fig. 6a based on the extended Taylor formulae, although the plate with $H/L = 0.1$ is predicted to be somewhat lighter. The main differences are the predicted optimal values of the design variables. For example, for plates with $H/L = 0.1$, $\mu \cong 2$ for the results in Fig. 8, while the prediction based on the extended Taylor formulae have $\mu \cong 1$. Compared to the extended approach, the simplified approach predicts significantly thinner faces counterbalanced by a heavier core. Moreover, both constraints, deflection and shear-off, are active in the simplified approach, while only the deflection constraint is active in the extended approach. If the shear-off constraint were removed, the simplified approach would predict even thinner faces. Differences for the fully optimized plates are not as large. The simplified approach has $H/L \cong 0.35$ and $\mu \cong 1.5$ compared with $H/L \cong 0.3$ and $\mu \cong 2$ for the extended approach, with both deflection and shear-off active in each approach.

In summary, some important differences emerge between analyses based on the simplified versus the extended Taylor fluid-structure interaction formulae, particularly with respect to the

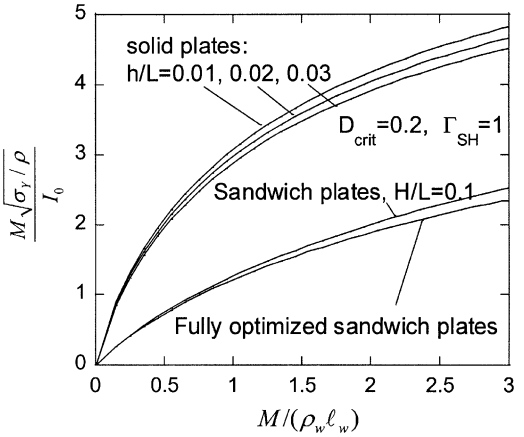

Fig. 8. Optimized square honeycomb core sandwich plates for water pulses based on the simplified approach that neglects the effect of the core on the motion of the face sheet towards the pulse in Stage I. These results are independent of the plate half-width, L. The plates with $H/L = 0.1$ are optimized with respect to μ with the result that $\mu \cong 2$ over the range shown. Both H/L and μ are varied in the full optimization with the result $H/L \cong 0.35$ and $\mu \cong 1.5$ over the entire range. These results can be compared with those in Fig. 6a based on the extended approach that accounts for the core in Stage I.

optimal design variables. In Section 8.3, it will be shown that there are significant changes in the optimal design variables when the plate dimension L is reduced by an order of magnitude. These changes are missed altogether by the simplified approach since L does not appear in the formulation, apart from its appearance in the dimensionless design variable. Nevertheless, overall trends for the mass of a fully optimized plate as a function of the free-field momentum of the pulse are reasonably well captured by the simplified Taylor analysis when shear-off is added as a constraint, and the benefit of sandwich over monolithic construction is realistically revealed.

8. Additional trends and issues

The present approach, although based on relatively simple approximations governing the deformation of the plates, has the advantage that it identifies a small set of dimensionless parameters that characterize the performance and design of sandwich plates against impulse loadings in water and air environments. The benefit of sandwich plates over equal mass solid plates is clearly delineated by the study. Moreover, it is significant that sandwich plates with square honeycomb cores with normalized thickness, $H/L = 0.1$, can be almost as effective as designs where no constraints are placed on core thickness. This is significant since fully optimized plates have cores that are probably too thick for many applications. The present analysis implies that minimum weight plates designed against impulses in water with square honeycomb cores and $H/L = 0.1$ have roughly one third of their mass allocated to the core. Additional parametric trends and issues are readily explored, as will be illustrated below. Verification of predictions of the approach will require finite element simulations that account for strain hardening, material

rate dependence, fracture and detailed nonlinear response of the core, including inertial effects, and fluid-structure interaction. Nevertheless, the measures of performance presented here and the trends outlined should serve to guide more detailed studies. Further implications of the model are discussed below.

8.1. The role of shear-off resistance, Γ_{SH}

In the numerical examples presented above, the choice $\Gamma_{SH} = 1$ was made on the basis of minimal empirical data, as noted in Section 6. The shear-off constraint comes into play in the design of the fully optimized sandwich plates, but not for solid plates or sandwich plates with $H/L = 0.1$ (with $D_{crit} = 0.2$ and $\Gamma_{SH} = 1$). The effect of shear-off resistance, Γ_{SH}, on plates with $H/L = 0.1$ and $\mu = 1$ is illustrated in Fig. 9. For $\Gamma_{SH} > 0.7$, the shear-off constraint is inactive and Γ_{SH} has no influence. However, smaller Γ_{SH} results in shear-off being the controlling constraint with the consequence that the plates are heavier. Over the range of Γ_{SH} in Fig. 9, the solid plate remains unaffected by shear-off. The main conclusion to be drawn is that shear-off is likely to be an important consideration in the design of sandwich plates against impulsive water loads because optimization tends to favor sandwich plates with thin faces that are more susceptible to shear-off. Basic experimental work is needed to establish shear-off resistance, Γ_{SH}. Design of support conditions to alleviate face sheet shear-off is possible, both at the ends of the plate and at the junctions with core webs.

8.2. Designing for air or water environments

Some difference emerged between designs in air and water environments. For example, for sandwich plates with normalized core thickness fixed at $H/L = 0.1$, the best performing plates in air have $\mu \cong 0.5$ while those in water have $\mu \cong 1$. Fortunately, each design is effective in both

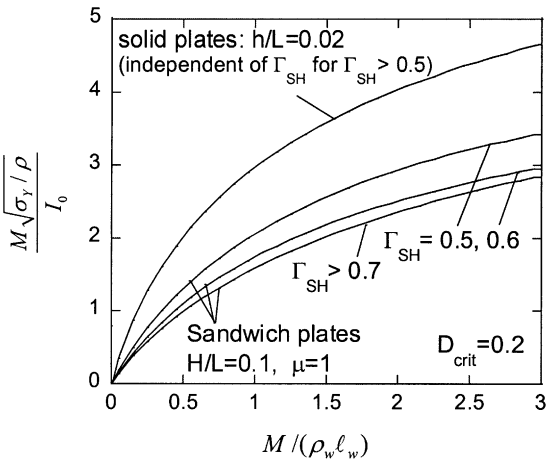

Fig. 9. The effect of shear-off resistance, Γ_{SH}, on sandwich plates with square honeycomb cores with $H/L = 0.1$, $\mu = 1$ and $C_L = 0.015$.

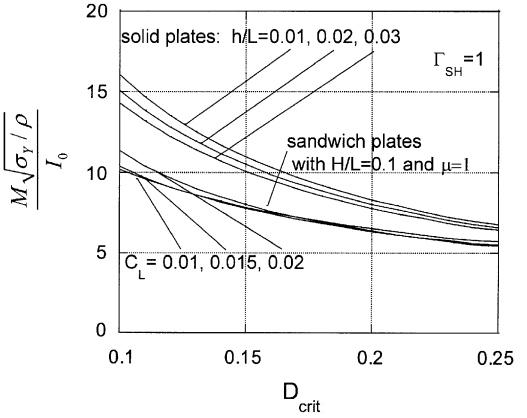

Fig. 10. An example demonstrating the good performance against impulses in air of sandwich plates with square honeycomb cores designed for impulses in water ($H/L = 0.1$ and $\mu = 1$). The performance for plates specifically designed for air impulses is plotted in Fig. 5.

environments. For example, the performance of the plate with $H/L = 0.1$ and $\mu = 1$ subject to an impulse in air (Fig. 10) is nearly as good as that of the optimized plate in air with $H/L = 0.1$ in Fig. 5.

8.3. Scaling considerations for small test specimens

The half-width of a sandwich plate, L, enters only through the parameter C_L defined in Eq. (23). As previously emphasized, the numerical values of C_L used to generate the curves in the figures presented thus far apply to plates whose half-widths lengths are typically on the order of 1 m for pulses with $t_0 = 10^{-4}$ s. Suppose one is interested in conducting laboratory scale tests on specimens of the same material as used in a full scale plate structure, but scaled down in all dimensions by a factor often such that L is on the order of 0.1 m. The most straightforward procedure which preserves the applicability of all the curves plotted above is to reduce the pulse time, t_0, by a factor of ten. Doing so leaves C_L unchanged, as well as the *relative* times associated with the three stages: t_C/t_0, t_{II}/t_0 and t_{III}/t_0. H. Espinosa and co-workers (private communication) have reduced both size and pulse time in developing a laboratory-scale testing facility. A drawback of this approach is that strain-rates increase in inverse proportion to the reduction in size and pulse time. Thus, material strain rate dependence, which has not taken into account in this paper, will not be scaled correctly.

Alternatively, if the pulse time t_0 is unchanged and only dimensions are scaled down by a factor of ten, the strain-rates in Stages I and II are unchanged but the curves presented in Figs. 4–8 are invalid because C_L in Eq. (23) is increased by a factor of ten. New results must be computed. An example is presented in Fig. 11 for steel plates in water with $L = 0.1$ m, $\sigma_Y = 200$ MPa, $\rho = 8000\,\mathrm{kg/m^3}$ and $t_0 = 10^{-4}$ s ($C_L = 0.158$). The relevant range of normalized plate mass becomes $0 < M/\rho_w \ell_w < 0.3$. Qualitative trends seen for the full-scale plates persist, but quantitative differences arise, particularly with respect to the distribution of mass in the faces and the core. For small-scale plates with $H/L = 0.1$, the minimum mass plates in Fig. 11 have $\mu \cong 0.2$ (with $\bar{\varepsilon}_c \cong 0.3$), while those with $H/L = 0.3$ have $\mu \cong 0.7$ (with $\bar{\varepsilon}_c \cong 0.2$). Thus, a well-designed

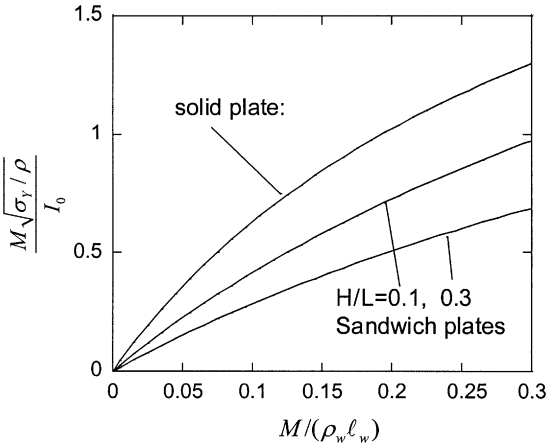

Fig. 11. Normalized mass of small-scale steel plates having half-width of $L = 0.1$ m designed against impulses in water with $t_0 = 10^{-4}$ s. Full details specified in the text. These predictions can be compared with the corresponding results for full-scale plates ($L \simeq 1$ m) in Fig. 6.

small-scale plate has a substantially lower fraction of its mass allocated to the core. In addition, the benefit of the sandwich plate relative to the solid plate is not quite as large as for the full-scale plate. Lastly, a clear separation of the time scales becomes questionable for these small scale plates, since $t_{III} \sim L/\sqrt{\rho/\sigma_Y} = 6.3 \times 10^{-4}$ s.

8.4. The role of core strength

As Deshpande and Fleck [6] have observed, the role of core strength on the performance of sandwich plates is complicated in water blasts. High core strength limits core crush, enables energy absorption, and maintains the bending strength of the plate, but it adversely results in more momentum imparted to the plate (Fig. 1a). The trade-off between these two factors is not obvious. Some insight into the competing effects can be obtained from Fig. 12a and b for full-scale plates ($L \approx 1$ m) designed against impulses in water. In Fig. 12a, both core thickness and relative core mass are fixed at $H/L = 0.1$ and $\mu = 1$, respectively, but the pair of factors, λ_c and λ_S, characterizing the crushing strength and in-plane stretching strength of the core are varied. Recall that $\lambda_c = 1$ and $\lambda_S = 1/2$ for square honeycomb cores, which are generally regarded as the strongest possible cores. Small reductions in λ_c and λ_S have fairly small effect on the minimum weight, but a strength reduction with $\lambda_c = 1/4$ and $\lambda_S = 1/8$ starts to become significant, and larger reductions reflecting the strength of foam metal cores would lead to even larger weight increases.

The example in Fig. 12a is not conclusive since it does not consider any redesign of the sandwich plate to take advantage of the lower strength of the core. Fig. 12b shows the outcome of redesign for each pair of strength factors, λ_c and λ_S, for plates with $H/L = 0.1$ but now having M minimized with respect to μ. The dependence of M for the redesigned plate on the core strength is surprisingly weak, and, in fact, a range of $M/\rho_w \ell_w$ exists where cores with lower strength have slightly lower weight than the high strength cores. There is, however, a significant hidden penalty to be paid for this reduction in core strength. As noted earlier, plates with strong cores ($\lambda_c = 1$,

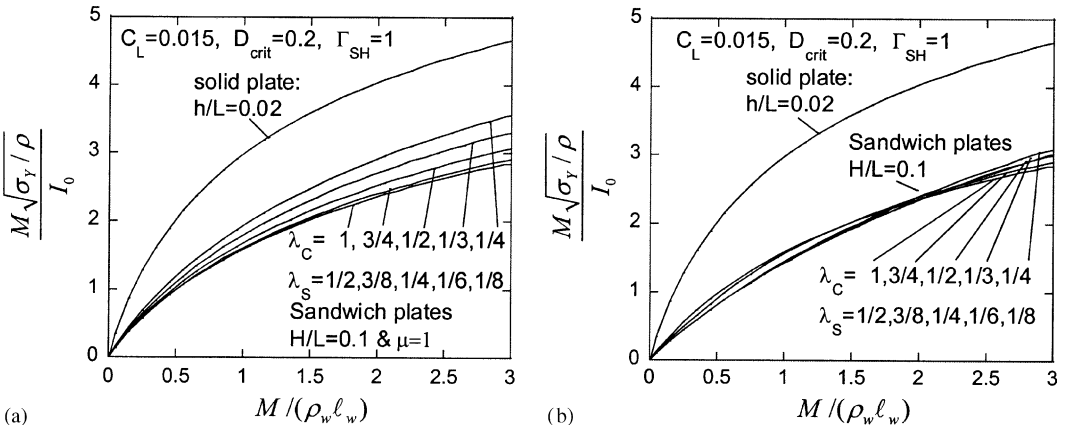

Fig. 12. The influence of core strength on normalized mass of the sandwich plates. The factors governing crushing strength, λ_c, and stretching strength, λ_S, are reduced in proportion. (a) Plates with $H/L = 0.1$ and $\mu = 1$. (b) Plates with $H/L = 0.1$ but redesigned with respect to μ for each pair of strength factors. The plates with reduced core strength have much larger proportion of mass allocated to the core.

$\lambda_S = 1/2$) have about $\frac{1}{3}$ of their mass is in the core ($\mu \cong 1$). Sandwich plates with weaker cores in Fig. 12b require a much higher fraction of their mass in the core. Plates with the weakest cores ($\lambda_c = 1/4$ and $\lambda_S = 1/8$) have μ between 4 and 6 such that the core comprises about $\frac{3}{4}$ of the plate mass. Even a modest reduction in strength to $\lambda_c = 3/4$ and $\lambda_S = 3/8$ significantly increases the fraction of mass in the core required if the plate is to perform as well as the plate with the square honeycomb core. Compared to plates with square honeycomb cores, plates with low strength cores would necessarily have very thin face sheets. Considerations not envisioned in the design constraints employed here may exclude very thin faces, such as a dramatically lowered overall bending stiffness and strength as well as lower penetration resistance. In conclusion, while it appears that a slight weight advantage for plates with lower core strength may be possible for water blasts, the distribution of mass between core and faces probably make these designs unacceptable.

The situation for air blasts is more clear-cut since the core has no effect on the momentum transfer. Lower core strength results in decidedly higher plate weight.

8.5. Core yield versus elastic buckling

Although not stated explicitly, the model used above is premised on the assumption that plastic yielding occurs prior to elastic bucking in the core in Stage II. Were that not the case, the assumption underlying the determination of σ_Y^c in Eq. (23) would not be valid. The crushing strain of the core would be underestimated, possibly significantly so, because cores that buckle elastically are not nearly as effect in absorbing energy as those that yield plastically before buckling [14]. To illustrate when this comes into play, consider square honeycomb cores with $B/H = 1$ and web thickness h_c. A lower bound to the compressive bucking stress of the web is the buckling stress of a simply supported square plate of width B: $\sigma_{cr} = \pi^2 E(h_c/B)^2/[3(1-\nu^2)]$, where E is Young's modulus and ν is Poisson's ratio. The condition for yield to precede buckling

is $\pi h_c/B > \sqrt{3(1-\nu^2)\sigma_Y/E}$ or, equivalently, $R_c > (2/\pi)\sqrt{3(1-\nu^2)\sigma_Y/E}$. This condition can be re-expressed as

$$\frac{M}{\rho_w \ell_w} > \frac{(2+\mu)}{\pi\mu}\frac{\rho H}{\rho_w \ell_w}\sqrt{\frac{3(1-\nu^2)\sigma_Y}{E}} \text{ (square honeycomb core, } B/H = 1). \tag{24}$$

For steel plates with $\sigma_Y = 200\,\text{MPa}$, $L = 1\,\text{m}$, $H/L = 0.1$ and $\mu = 1$, condition (24) for yield before bucking is $M/\rho_w \ell_w > 0.3$. Thus, the results in Fig. 5 for $M/\rho_w \ell_w < 0.3$ are likely to underestimate the plate mass. Buckling versus yield is an additional consideration that should be taken into account in the design process.

9. Concluding remarks

The trends presented in this paper are limited in several respects. Firstly, they are based on simple approximations to the plate responses. Secondly, they ignore influences such as strain hardening, material strain-rate effects, specific fracture modes and dynamic strengthening of the core. To surmount these limitations, more elaborate, computationally intensive, finite element simulations will be required. Nevertheless, the approach highlights trends that govern the design of sandwich plates against dynamic impulsive loads. A small set of the most important dimensionless parameters has been identified. In Section 8, the model has been employed to explore a number of open issues related to the design of high performance metal sandwich plates. Theoretical efforts directed at a better understanding of fracture and shear-off have been initiated [11,15]. In addition to detailed numerical studies, experimental work is needed to establish requirements that exclude face sheet shear-off. Finally, further large-scale calculations are needed to provide confidence, or to improve, the fluid-structure interaction approximations employed here. Much of the benefit of sandwich plates over solid plates in a water environment rests on fluid-structure interaction and, as revealed by the present study, optimal designs depend on the details of this interaction.

Acknowledgements

This work was supported in part by ONR Grant N00014-02-1-700 and in part by the Division of Engineering and Applied Sciences, Harvard University. Discussions with T. Belytschko, V. S. Deshpande, A. G. Evans, N. A. Fleck, H. Wadley and L. Wegner are acknowledged.

Appendix A. Fluid–structure analysis for sandwich plates

The one-dimensional analysis of Taylor's [2,3] acoustic model of fluid–plate interaction is extended to sandwich plates with cores modeled as perfectly plastic with a compressive yield stress, σ_Y^c. The solution is valid until the instant when cavitation first occurs in the fluid. At this instant, the momentum/area in the faces and core are determined and subsequently used to establish the initial conditions for Stages II and III, as described in the body of the paper. The face

sheet impacted by the pulse is modeled as a plane of concentrated mass/area, m_f, whose motion is resisted by the yielding core. Let $\rho(x,t)$ be the pressure in the fluid and locate the plate at $x=0$, with the pulse first impacting the face at $t=0$. The free-field pulse is that assumed by Taylor: $p=p_0 e^{\xi}$ for $\xi \equiv (x-c_w t)/\ell_w \leqslant 0$, and $p=0$ for $\xi>0$, with c_w as the wave speed in the fluid, $\ell_w = c_w t_0$, and t_0 as the pulse period. The displacement $u(x,t)$ must satisfy the equation of motion of the face ($x=0$)

$$m_f u_{,tt} = p - \sigma_Y^c. \tag{A.1}$$

With $\zeta = (x+c_w t)/\ell_w$, the solution is

$$u = \frac{p_0 \ell_w}{E_w}\,[(1-e^{\xi}) + g(\zeta)], \tag{A.2}$$

where E_w is the modulus governing uniaxial compressive strains in the fluid such that $c_w = \sqrt{E_w/\rho_w}$. The reflected component of the wave is given by

$$g(\zeta) = 1 + \frac{\sigma_Y^c}{p_0}\left(\frac{1}{\beta}-\zeta\right) - \left(\frac{2}{1-\beta}+\frac{\sigma_Y^c}{p_0\beta}\right)e^{-\beta\zeta} + \left(\frac{1+\beta}{1-\beta}\right)e^{-\zeta}, \quad \zeta>0 \tag{A.3}$$

and $g=0$, $\zeta<0$ with $\beta = \rho_w \ell_w/m_f$.

The onset of cavitation is assumed to occur when p first becomes negative. If $\sigma_Y^c/p_0 = 0$, onset occurs at the fluid-face sheet interface (Taylor's limit), while if $\sigma_Y^c/p_0 > 0$, it occurs in the fluid at (x_C, t_C) where simultaneously $p=0$ and $p_{,x}=0$. With $\zeta_C = (x_C + c_w t_C)/\ell_w$ and $\xi_C = (x_C - c_w t_C)/\ell_w$,

$$(1+\beta)\left(2\beta + (1-\beta)\,\frac{\sigma_Y^c}{p_0}\right)e^{-\beta\zeta_C} - 2(1+\beta)e^{-\zeta_C} - (1-\beta)\,\frac{\sigma_Y^c}{p_0} = 0 \tag{A.4}$$

and $e^{\xi_C} = g'(\zeta_C)$. The mass/area of the fluid layer between the plane of cavitation and the face sheet is $m_w = \rho_w |x_C|$ from which it follows that $r_w = m_w/m_f = \rho_w |x_C|/\rho_f h_f$ which is displayed in Fig. 1b. The velocity of the face at the onset of cavitation is

$$V_0 = \frac{p_0 c_w}{E_w}\,(e^{-t_C/t_0} + g'(t_C/t_0)). \tag{A.5}$$

The velocity of the fluid in the added fluid layer, $|x_C| < x < 0$, is essentially uniform at $t=t_C$ and equal to V_0. Assuming this, the momentum/area in the face and added layer at the onset of cavitation is

$$\frac{I_F}{I_0} = \frac{(1+r_w)}{\beta}\,(e^{-t_C/t_0} + g'(t_C/t_0)). \tag{A.6}$$

The momentum/area, I_B, transferred to the core and the back face sheet at cavitation is precisely $\sigma_Y^c t_C$, such that $I_B/I_0 = (\sigma_Y^c/p_0)(t_C/t_0)$, which is presented in Fig. 1c. The total momentum/area, including that of the added water layer, is given by $I_T = I_F + I_B$ and is presented in Fig. 1a. Formulae (1), which are linear in σ_Y^c/p_0, are approximations obtained from the solution given above. For the results in Fig. 1 with $\sigma_Y^c/p_0 \leqslant 0.15$, the exact results from the above solution are virtually indistinguishable from Eq. (1).

Assuming t_0 is sufficiently small compared to the response time for bending and stretching of the plate, there are two main reasons why the above model may not accurately capture the

fluid–structure interaction. Firstly, dynamic effects associated with the mass of the core have been neglected. A core with a compressive yield stress that is independent of the strain and strain-rate is highly idealized. Deshpande and Fleck [6] adopted a perfectly plastic core with a compaction limit, and they analyzed the progression of the plastic wave through the core during the fluid–structure interaction. At large impulses, an additional parameter emerges associated with full compaction of the core, depending nonlinearly on the amplitude of the free-field momentum itself. A compaction limit is not accounted for in the present model. Another reason for error is closure of the cavitation gap subsequent to the onset of cavitation. If the gap closes, additional pressure will be exerted on the plate and more momentum will be transferred to it than the above prediction at $t = t_C$. Analysis [6] reveals that the cavitation gap does close. However, except when σ_Y^c/p_0 is fairly large and/or when the nonlinear dependence on the impulse associated with full compaction is important, the additional momentum imparted is small compared to I_T given above. Checks against the analysis in [6] indicate that the results presented in the body of the paper fall within the range where the errors of the extended fluid–structure formulas (1) should be small. In all cases presented, $\sigma_Y^c/p_0 \leqslant 0.15$. Moreover, crushing strains in the square honeycomb cores are not larger than 0.3, and in most instances even smaller, and therefore well below compaction limits at least in an average sense.

References

[1] Johnson W, Reid SR. Metallic energy dissipating systems. Applied Mechanics Reviews 1978;31:277–288, Updated 1986;39:315–9.
[2] Taylor GI. The pressure and impulse of submarine explosion waves on plates. The scientific papers of G.I. Taylor, vol. III. Cambridge: Cambridge University Press; 1963. p. 287–303.
[3] Cole RH. Underwater explosions. Princeton: Princeton University Press; 1948.
[4] Fleck NA, Deshpande VS. The resistance of clamped sandwich beams to shock loading. Journal of Applied Mechanics 2004;71:386–401.
[5] Xue Z, Hutchinson JW. A comparative study of impulse-resistant metallic sandwich plates. International Journal of Impact Engineering 2004;30:1283–305.
[6] Deshpande VS, Fleck NA. One-dimensional shock response of sandwich plates 2005; submitted for publication.
[7] Rabczuk T, Kim JY, Samaniego E, Belytschko T. Homogenization of sandwich structures. International Journal of Numerical Methods in Engineering 2004;61:1009–27.
[8] Rathbun HJ, Radford DD, Xue Z, He MY, Yang J, Deshpande VS, Fleck NA, Hutchinson JW, Zok FW, Evans AG. A dynamic probe for validating simulations of shock loaded metallic sandwich panels. International Journal of Solids and Structures 2005, in press.
[9] Xue Z, Hutchinson JW. Preliminary assessment of sandwich plates subject to blast loading. International Journal of Mechanical Science 2003;45:687–705.
[10] Jones N. Structural impact. Cambridge: Cambridge University Press; 1989.
[11] XueZ. work in progress.
[12] Vaughn D, Canning M, Hutchinson JW. Coupled plastic wave propagation and column buckling. Journal of Applied Mechanics 2005;72:139–46.
[13] Menkes SB, Opat HJ. Broken beams. Experimental Mechanics 1973;13:480–6.
[14] Cote F, Deshpande VS, Fleck NA, Evans AG. The out-of-plane compressive behavior of metallic honeycombs. Materials Science & Engineering A 2004;380:272–80.
[15] Alves M, Jones N. Impact failure of beams using damage mechanics: Part I- analytical model, Part II-application. International Journal of Impact Engineering 2002;27:837–861, 863–90.